Light-Induced Selective Deposition of Au Nanoparticles on Single-Wall Carbon Nanotubes

Mildred Quintana,[†] Xiaoxing Ke,[‡] Gustaaf Van Tendeloo,[‡] Moreno Meneghetti,[§] Carla Bittencourt,[⊥] and Maurizio Prato[†,*]

[†]Center of Excellence on Nanostructured Materials (CENMAT) and INSTM, Unit of Trieste, Dipartimento di Scienze Farmaceutiche, Università degli Studi di Trieste, Piazzale Europa 1, I-34127, Trieste, Italia, [‡]Electron Microscopy for Materials Science, Universiteit Antwerpen, Gronenborgerlaan 171, 2020 Antwerp, Belgium, [§]Dipartimento di Scienze Chimiche, Università di Padova, Via Marzolo 1, 35131 Padova, Italy, and [⊥]Chimie Inorganique et Analytique, Univeristé de Mons, Rue du Parc 20, 7000 Mons, Belgium

ABSTRACT Novel applications of single-walled carbon nanotubes (SWNT) rely on the development of new strategies to make them easier to handle without affecting their structural properties. In this work, we have selectively deposited Au nanoparticles (Au NP) on SWNT assisted by UV light irradiation. XPS analysis and UV—vis spectroscopy indicate that the deposition occurs at the defects generated after oxidation of the SWNT. By addition of *n*-dodecylthiol, the separation of oxidized tubes with Au NP (Au-ox-SWNT) from tubes devoid of Au NP (bare tubes, b-SWNT) was achieved. Raman and UV—vis—NIR spectra indicate that UV irradiation induces a faster nucleation of Au NP on metallic SWNT. This new technique can be useful for the preparation of nanohybrid composites with enhanced properties, as increased thermal stability, and to obtain purified SWNT.

KEYWORDS: single-walled carbon nanotubes · gold nanoparticles · UV light irradiation · nanocomposites

The motivation of understanding how nanotubes interact with light is both fundamental and applied. Nanotubes may some day be used as near-infrared fluorophores,[1] biological tags,[2] sensors,[3] components for photovoltaics,[4] and optical communications systems.[5] However, single-walled carbon nanotubes (SWNT) are synthesized as heterogeneous samples, composed of tubes of different chirality, diameter, and length.[6] As a result, SWNT samples are mixtures of semiconducting and metallic tubes, presenting very different photoelectronic characteristics. A promising approach to elucidate the photophysical behavior of SWNT in the bundles is the deposition of metal nanoparticles (NP) assisted by UV light irradiation, since recombination of photoexcited carriers directly competes with the ability of tubes to create electron—hole (e—h) pairs. The small Fermi velocity and low dielectric constant in SWNT suggest that high-energy photons should efficiently generate these pairs,[7] which finally can induce the nucleation of metal NP. For SWNT, the band gap energy E_{nn}, is the energy required to generate an e—h pair. The UV light-assisted deposition of metal NP may give some clues to discern between the photophysics response of metallic and semiconducting SWNT in the bundles, since they present different band gap energies, E_{11}, E_{22} for semiconducting and E_{11} for metallic SWNT. The detailed understanding of the mechanism involved in the NP deposition by UV light irradiation on SWNT is a challenge, as many factors are involved. Previous studies have demonstrated that light-assisted oxidations with H_2O_2 exhibit dependence on the diameter and band gap.[8] Photohydroxylation of first semiconducting and then small diameter metallic SWNT was produced after 254 nm irradiation in acidic, neutral, and basic aqueous solutions at ambient and elevated temperatures.[9] The use of UV light irradiation can be a valuable tool for creating SWNT composite materials. In fact, it has been observed that direct UV light irradiation of SWNT deposited on a surface induces photo-cross-linking of the tubes, improving the electrical conductivity and the mechanical properties of the bundles.[10]

Metal NP supported on the surface of carbon nanotubes have attracted much interest in the catalytic community due to their potential use as hydrogen sensors,[11] catalysts,[12] and direct methanol fuel cells.[13] Metal NP ranging in diameter from roughly 1 to 50 nm exhibit physical and chemical properties that are intermediate between those of the isolated atom and the bulk material. Catalyst performance on SWNT composites strongly depends on particle size because the surface structure and electronic

*Address correspondence to prato@units.it.

Received for review May 27, 2010 and accepted September 10, 2010.

Published online September 24, 2010.
10.1021/nn101183y

properties change greatly with this size range.[14]

In the present work, we have attached Au NP to oxygenated groups produced on the surface of SWNT by chemical oxidation, following the reduction of $HAuCl_4$ to form NP under UV light irradiation in the presence of citric acid.[15] SWNT samples with different degrees of oxidation were produced by two different techniques, mild purification in nitric acid (**ox-SWNT**)[16] and treated in piranha solution (**cut-SWNT**),[17] which result in highly oxidized material. Our results show that oxidized defects at sidewalls of SWNT play an essential role as nucleation sites for the Au NP formation and later on their stabilization. This new protocol allows also the separation of nanotubes with deposited NP (**Au-ox-SWNT**) from the tubes devoid of NP (bare tubes, **b-SWNT**). The procedure can be useful for both the preparation of nanohybrid composites, **Au-ox-SWNT**, with enhanced properties as high thermal stability, and to obtain purified SWNT, **b-SWNT**. Our results also motivate the future understanding of how CNTs interact with light at both fundamental and applied levels and provide some clues about the interaction between SWNT and metal NP,[18] demonstrating that oxidized defects at the SWNT surface are relevant in the synthesis of composite materials.

RESULTS AND DISCUSSION

Deoxygenated water−methanol dispersions of **ox-SWNT** or **cut-SWNT**, with the addition of citric acid were exposed to UV light irradiation during 1 h using different concentrations of chloroauric acid (0.05, 1, and 3 mM). Dispersions were filtered and washed several times with deionized water. The formation of Au nanoparticles was followed by UV−vis−NIR spectrophotometry. Through TEM and UV−vis−NIR studies, we observed that the filtered solutions of SWNT treated with UV light did not contain NP, which indicates that Au NP only grew and remained attached at the walls of SWNT. To verify this, the chemical changes induced in the SWNT surface were evaluated through photoelectron spectroscopy (XPS). The relative amount of oxygen atoms grafted at the surface of the **cut-SWNT** was evaluated to be 18% higher than in **ox-SWNT**. Figure 1 shows the XPS spectra for the C 1s peak recorded on **p-SWNT**, **ox-SWNT**, and **cut-SWNT**, before and after Au deposition. In pristine samples, the C 1s spectrum has its main features at 284.3 eV and a secondary, the core-energy-loss spectrum, corresponding to a p plasmon excitation centered at 291 eV.[19] The shoulder at the high-energy side of the C 1s peak for the **ox-SWNT** is generated by photoelectrons emitted from C atoms in oxygenated groups: hydroxyl (component centered at 286.2 eV), carbonyl (287.2 eV), and carboxyl groups (288.9 eV).[20] From the variation in the relative intensity of the components forming this broad structure in the spectrum recorded for the **cut-SWNT** sample, it can be suggested that the treatment in piranha solution reduces the variety in the type of oxygenated groups at the SWNT surface, pushing the reaction toward higher oxidation states, such as the carboxyl groups.[21]

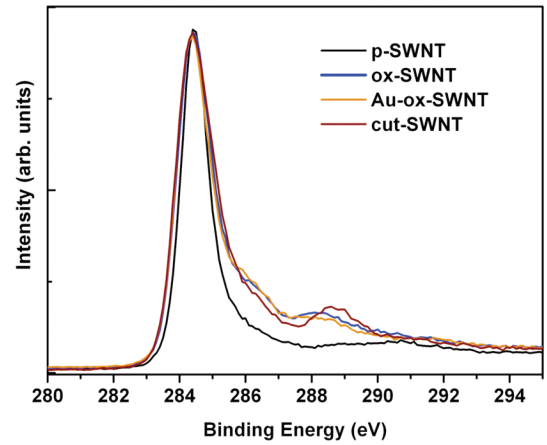

Figure 1. XPS spectra for the C 1s peak recorded on p-SWNT, ox-SWNT, and cut-SWNT, before and after Au deposition.

Comparison of the line shapes of the C 1s XPS spectrum recorded after the Au deposition shows that the C 1s satellite peaks due to oxygenated-groups are slightly reduced. Two effects can contribute to this observed reduction. First photoelectrons emitted from C atoms beneath the Au particles will experience inelastic losses when passing through the metal, and thus no longer contribute to the C 1s main peak. If Au NP selectively cover oxygen-rich areas, thus the intensity from oxygen-related C 1s satellite peaks will be selectively reduced. A second possible cause for the reduction in oxygen-related C 1s satellite peaks in the XPS spectra is the formation of O−Au bonds. C−O−Au bonding will change the screening of the C−O bonds thereby changing the binding energy of their C 1s levels.

On the basis of previous work reported in the literature, which shows the essential role that defects play on gold nucleation at graphitic[22,23] and metal−oxide surfaces,[24] as well as on the results of our current experiments, we believe that Au clusters nucleate at oxidized defects on the SWNT surface and grow as a function of increasing gold concentration in the solution and UV light exposure time. We found that at lower Au concentrations in solution (0.05 mM), NP are deposited mainly on the tube walls and at the end of the small bundles, as shown in Figure 2, (endings of small bundles are indicated by arrows). It has been reported that oxidized vacancies at CNT-open tips prevent their closing;[25] our results suggest that these vacancies can be nucleation sites for NP.

At higher concentrations of Au in solution (1 and 3 mM), a nonuniform distribution of NP can be seen in Figure 3a−f. Samples prepared under different experimental conditions are shown: **Au-ox-SWNT** obtained from 1 mM $HAuCl_4$ solutions irradiated for 60 min, detailing a dispersion and a bundle, respectively (Figure 3a,b). As can be observed, Au NP are spherical and

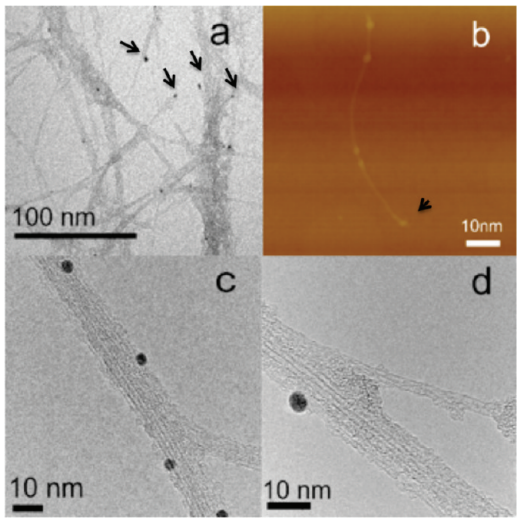

Figure 2. TEM (a), AFM (b), and HR-TEM (c and d) images of Au-ox-SWNT at low Au concentration (0.05 mM).

present an average size of 11 ± 5 nm. For the samples obtained with 3 mM concentration of $HAuCl_4$ and irradiated for the same time, the shape of NP seems to elongate; both the form factor and the size distribution are broader. This result is in agreement with the reported spontaneous metal NP formation on as-grown SWNT on SiO_2, which purely utilizes the redox potential difference between Au^{3+} or Pt^{2+} and the carbon nanotube.[26] These authors found that longer reaction times cause the formation of larger particles, but do not lead to any apparent increase in the density of particles at the tube surface. Even if the NP formation mechanism is different, the nucleation of the particles seems to occur selectively at the defects, that is, oxidized vacancies, in both, their case and our case.

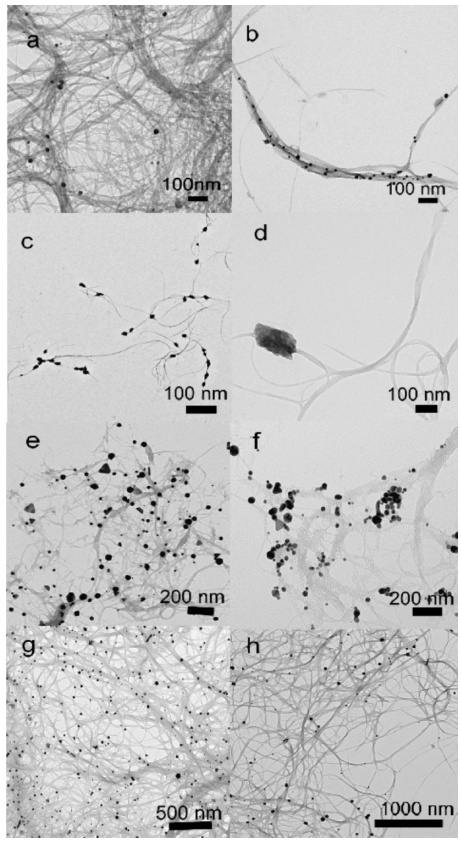

Figure 3. TEM pictures of Au-ox-SWNT: (a and b) 1 mM; (c−f) 3 mM. (g and h) Au-cut-SWNT.

A significant difference was observed between **ox-SWNT** and **cut-SWNT** loading at higher concentration of $HAuCl_4$ (3 mM). The NP size distribution on **Au-ox-SWNT** (65%, 11 ± 5 nm and 35%, 70 ± 5 nm) is broader and exhibits a bimodal structure when compared with that of **Au-cut-SWNT** (11 ± 5 nm). The amorphous carbon impurities, normally found in SWNT, were considerably reduced in the tubes treated in piranha solution, **cut-SWNT**. The purity of the tubes and the number of introduced defects might influence the NP deposition as observed in Figure 3 g,h. The chemical oxidation of SWNT can produce different types of defects: oxidative attack at the existing active sites such as sidewall functional groups, generation of additional active sites, and introduction of vacancies in the graphene layer. In addition, consumption of the graphene sidewalls around the vacancies of nanotube end shortens the tubes resulting in differently oxygenated-groups at the SWNT surface.[27] Suarez-Martinez *et al*. reported that the binding energy between a gold atom and an oxygenated defect will depend on the nature of the defect.[19] These authors showed that the binding energy of the gold atom to a pristine MWNT surface is 0.66 eV and will rise to 1.07 or 1.16 eV if the atom is next to an oxygenated vacancy or to an oxygenated divacancy respectively. Then the observed bimodal size distribution of gold particles formed at the surface of oxidized MWNT may be due to the presence of mainly two types of oxygenated defects. From the XPS spectra (Figure 1) the broad band at high binding energy, indicates that for oxidized samples there is a spread in the type of oxygenated-groups grafted at the SWNT surface while for the SWNT treated with the piranha solution the variety of this groups is reduced. Thus, we suggest that the bimodal size distribution in the **ox-SWNT** samples is due to the formation of different defects at the SWNT surface during the oxidation using nitric acid, while the monomodal size distribution in **cut-SWNT** results mainly from two factors. First the higher concentration of oxygen atoms grafted at the nanotube surface. This implies a large number of active sites for nanoparticle nucleation—in this case the rate of nucleation of nanopartcicles will be higher. The second factor is the presence of mainly one type of defect at the SWNT surface (carboxylic groups). At higher concentrations of $HAuCl_4$, a competitive process can results in the growth of the first nucleated NP: Au seed particles can act as catalysts for the final reduction to elemental gold under UV light irradiation.[28]

Diverse control experiments were carried out. To increase the dispersibility of **ox-SWNT**, SDS (1 wt %) was

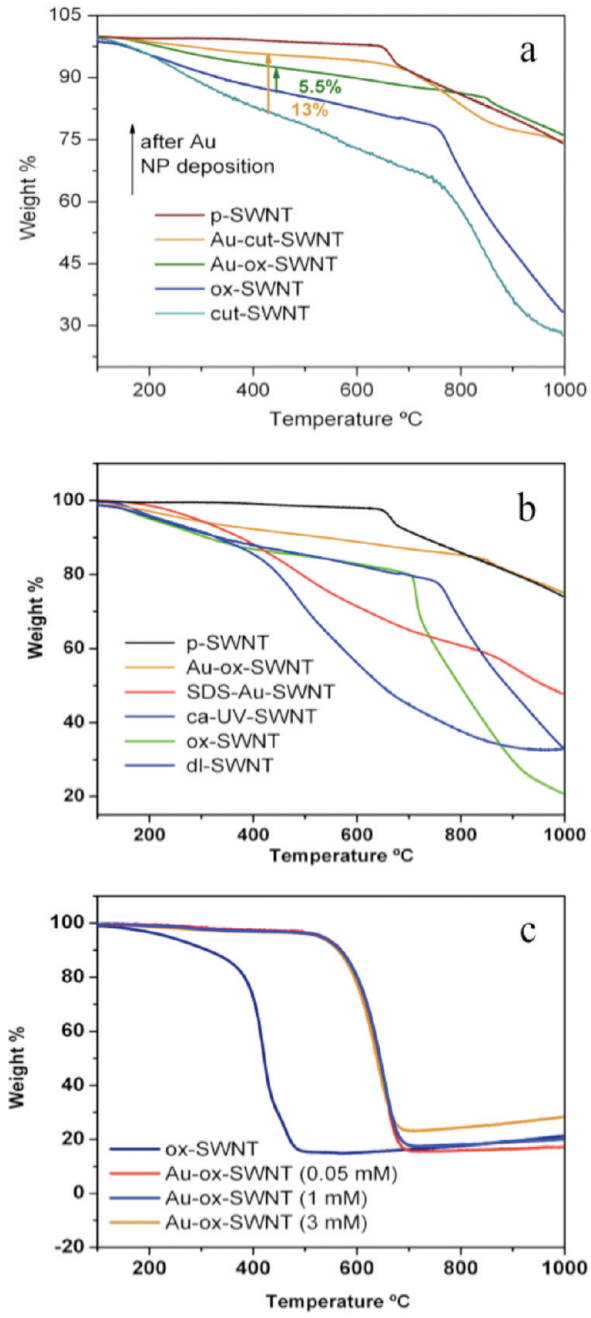

Figure 4. (a) Thermal gravimetric analysis in N, of ox-SWNT and cut-SWNT before and after Au NP deposition compared with p-SWNT. (b) TGA of p-SWNT, Au-ox-SWNT, SDS-Au-ox-SWNT, ca-Au-ox-SWNT, ox-SWNT and dl-Au-ox-SWNT in N. (c) TGA in air of ox-SWNT before and after Au NP depostion at the different concentration loadings of $HAuCl_4$.

added in selected cases before $HAuCl_4$ loading and UV light exposure. Several Au NP can be observed on the resulting material, **Au-SDS-ox-SWNT**. However it is difficult to discern whether they are directly deposited on SWNT or if they are trapped in the surfactant. Au NP deposited on SDS-treated SWNT can lead to partial interactions with the tube defects. Nevertheless, it was observed that after sonication in DMF, the NP were released from the SWNT, while in dispersions with no surfactant, the NP remained attached to the tubes even after sonication in the same experimental conditions. In a different control experiment, a sample of SWNT was not irradiated with UV light but only kept in daylight (**dl-Au-ox-SWNT**) at the same experimental conditions: the presence of Au could not be observed by TEM and EDX analysis, a demonstration that the UV light is required for NP growth.

Zhang, et.al. reported the depositon of Au NP on $-COO^-$ groups grafted at the MWNT surface using UV irradiation.[29] These authors showed that both the diameter of the MWNT and pH of the solutions affected the nucleation and growth of the NP. However, these authors do not present the chemical characterization of the different diameter oxidized MWNT. To our knowledge using the same experimental condition, the oxidation of MWNTs with different diameters leads to different amounts of oxygenated-groups grafted at the nanotube surface.[30] Then, the influence of the diameter of MWNT in the NP growth observed in this work might result from the degree of oxidation of the tubes. Our results corroborate that Au NP nucleate on the oxygenated-groups covalently attached to the tubes. In fact, in pristine, non-oxidized MWNT (**Au-MWNT**), the Au NPs formed during the reduction of $HAuCl_4$ grew in solution and not on the tubes. We attribute this observation to the reduced amount of oxygenated-groups in pristine MWNT. Also, in **cut-SWNT** treated for 9 h, instead of 1 h in piranha solution, (54 ± 5 nm length), the amount of deposited NP was not significant and particles were found mainly in solution. This indicates that the length, the surface reactivity, and the density of defects of SWNT are as well important factors. On the basis of our results, we suggest that extremely short tubes or highly damaged ones do not present the adequate photoresponse to generate a significant electron transport needed to turn defects into active gold nucleation sites.

TGA thermograms are in agreement with the increase of the thermal stability of the **Au-ox-SWNT** composites toward oxidation. A higher number of Au NP must be deposited on **cut-SWNT** compared with **ox-SWNT** in order to enhance their thermal stability, since **cut-SWNT** hold a higher number of oxygenated vacancies. TGA profiles of **ox-SWNT** and **cut-SWNT** are shown in Figure 4a. At 400 °C, the weight loss of **ox-SWNT** is 12%, while in **cut-SWNT** is 17%. After Au NP deposition under UV light irradiation, a considerable recovery of the thermal properties of the composite materials was observed. **Au-ox-SWNT** present now a weight loss of 6.5% showing a recovery of 5.5% when compared with the starting material (**ox-SWNT**). For **Au-cut-SWNT** the weight loss is 4%, which shows an increase of stability of about 13%. These results support the hypothesis that Au NP are deposited on oxygenated-defects on the differently treated SWNT. The presence of Au NP deposited on top of the defects might prevent their further oxidation, increasing the thermal stability of the resulting materials. Thermo-

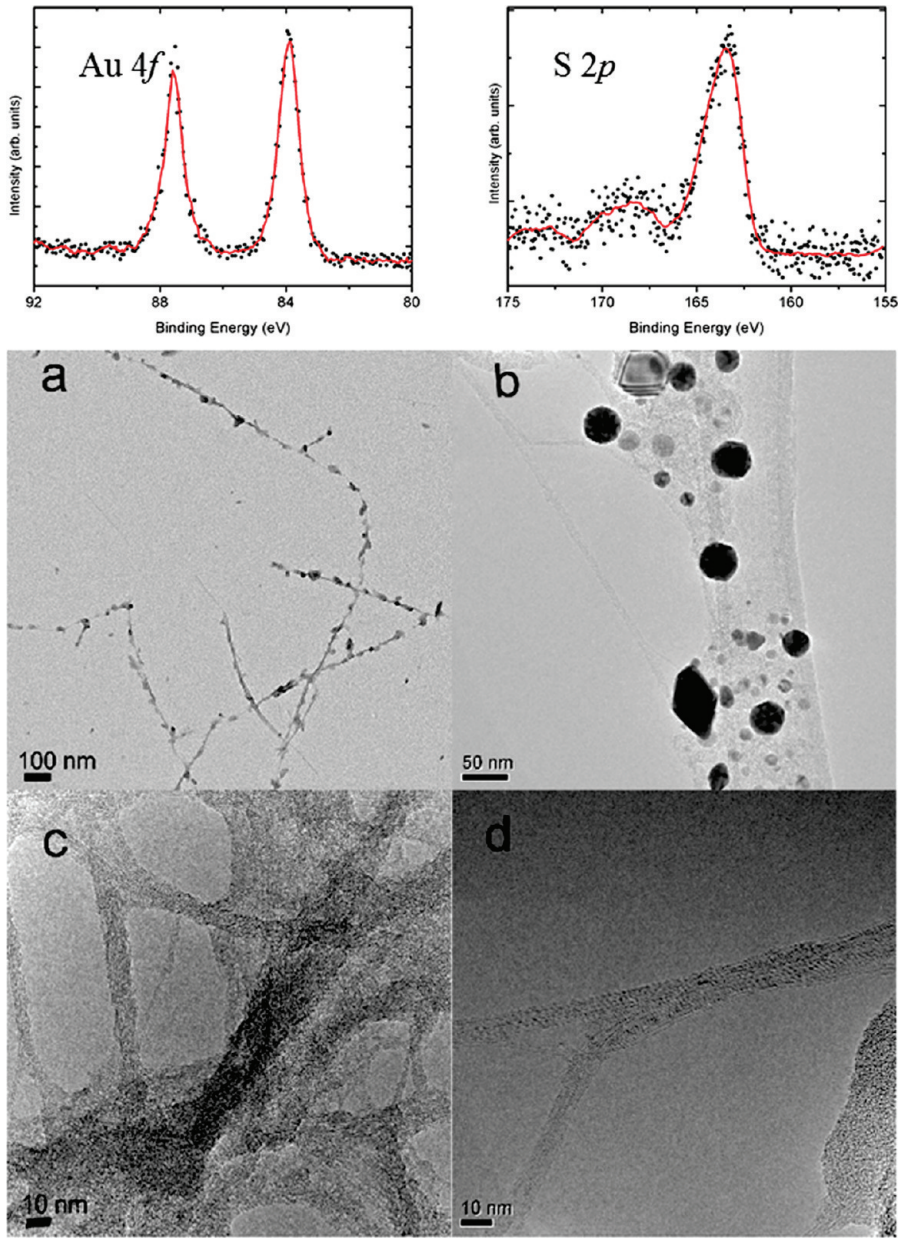

Figure 5. XPS spectra of Au 4f and S 2p region of Au-ox-SWNT. TEM and HR-TEM of **Au-ox-SWNT** (top) and **b-SWNT** (bottom) after separation by dodecylthiol.

grams of differently treated SWNT are shown in Figure 4b. At 850 °C the residual fractions of **Au-ox-SWNT** and **ox-SWNT** are 83% and 39%, respectively, while the **p-SWNT** residual fraction is 84%. This improved stability of **Au-ox-SWNT** was not observed in samples kept in daylight, **dl-Au-ox-SWNT**, in which case the samples began to decompose (~400 °C) even before **ox-SWNT** and the residual fraction at 850 °C is only 35%. This might be an indication of the physical adsorption of the diverse chemical species present in the solution. **SDS-Au-ox-SWNT** present a higher thermal resistance when compared to **ox-SWNT**, which might be the consequence of the grafting of the surfactant and of the partial defect interaction with deposited Au NP. It is interesting to note that the increase of the $HAuCl_4$ concentration or larger irradiation times do no considerably modify the TGA profiles. The same trend was observed in the TGA carried in air. The thermographs showed an increment in the thermal stability, **ox-SWNT** decompose at 423 °C, while **Au-ox-SWNT** at 630 °C. Both types of samples present the same characteristic profiles, indicating that the size distribution and shape of the deposited NP do not determinate the thermal stability increases. As expected, the residual fraction increases proportionally to the $HAuCl_4$ loading. This result corroborates that NP must be covering the oxidized vacancies, preventing the further oxidation of the graphene structure.

The separation of **Au-ox-SWNT** composites from tubes devoid of particles, bare tubes, **b-SWNT**, was per-

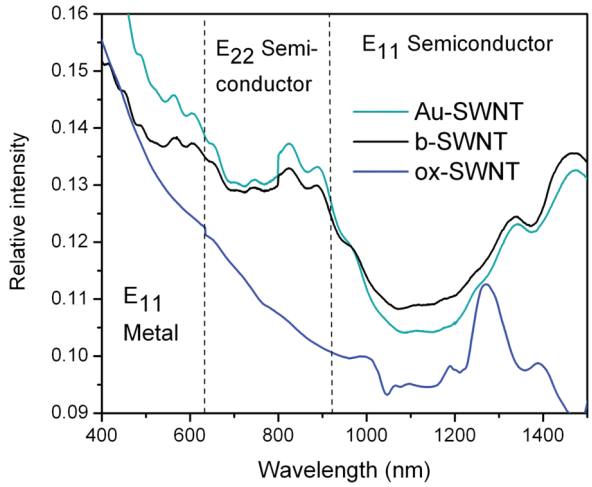

Figure 6. UV−vis−nIR spectra of b-SWNT and Au-ox-SWNT after separation are shown. E_{11} metal and E_{22} semiconductor regions develop the characteristic peaks after UV-light treatment.

formed based on Au interactions with thiols. In principle, after treatment with nitric acid, **ox-SWNT** will consist of oxidized tubes and intact nonoxidized tubes. Then, if the nucleation of Au NP occurs preferentially at the oxygenated sites, only the oxidized tubes will be covered with Au NP. Therefore, treatment of the **Au-ox-SWNT** with alkyl thiols should result into a different behavior allowing the possible separation of **Au-ox-SWNT** composite from **b-SWNT.** To this aim, *n*-dodecylthiol was added in a 1:1 volume ratio to 10 mg of **Au-ox-SWNT** composite prepared at 0.05 mM Au concentration, dispersed in DMF. Dodecylthiol self-assembles into a monolayer, covering the Au-NP surface (3D SAM).[31] The dispersion was sonicated until a homogeneous solution was obtained, and then centrifuged and left overnight. The whole procedure results in the formation of two clear liquid phases (DMF being the bottom phase) with two precipitated nanotube fractions, one at the interface containing **Au-ox-SWNT** and the second one

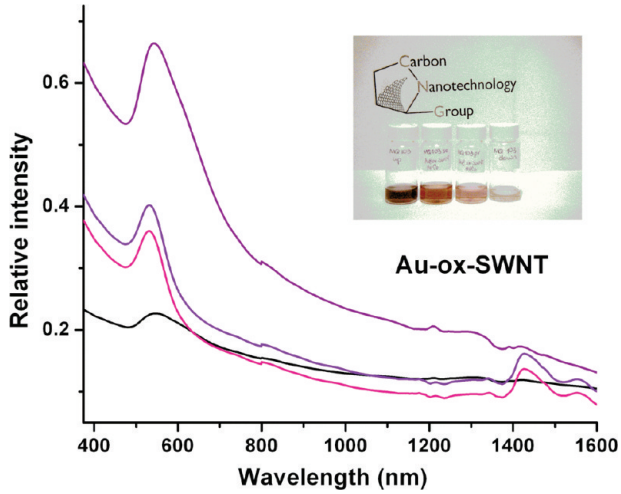

Figure 7. UV−vis−nIR spectra of Au-ox-SWNT prepared at high $HAuCl_4$ concentration in solution, after the addition of dodecylthiol. Different fractions can be obtained with higher concentration of NP.

at the bottom with **b-SWNT**. The two fractions were separated, filtered, and washed thoroughly. The SWNT−NP interactions in **Au-ox-SWNT** must be rather strong because neither the sonication treatment nor the addition of strong ligands such as thiols is sufficient to remove the particles from the tube surfaces. This fact confirms the previous observation that CNTs can be considered coordinating ligands during nanoparticle synthesis.[32] In all the separations (three identical experiments), the fraction ratios were approximately 1:4 **Au-ox-SWNT** to **b-SWNT** in weight. This result proves that purification in diluted nitric acid can be considered as a mild oxidant for SWNT.[33] Figure 5a,b displays TEM images of **Au-ox-SWNT** composites after separation. All the SWNT are covered with Au NP capped by dodecylthiol, while in Figure 5c,d, bundles of **b-SWNT** with no NP can be observed. **b-SWNT** remained in bundles because of the absence of NP and oxygenated vacancies. The Au 4f and S2p XPS spectra recorded on the **Au-ox-SWNT** samples are shown in Figure 5. The binding energy of the major component of Au 4f (Au $4f_{7/2}$ = 84 eV) is in agreement with results reported for alkanethiols assembled on gold nanoparticles.[34] The sulfur 2p peak presents two structures: the more intense at 162.8 eV binding energy generated by photoelectrons emitted from sulphur atoms in thiolate (S−Au) bond and the low intensity one at 168 eV that corresponds to the emission from sulphur atoms forming sulfones/sulfonates.[35] The presence of oxidized sulfur can be associated to an excess thiol derivative which was not removed by the washing protocols employed. In the case of **Au-cut-SWNT**, the same separation was not possible, because the presence of a higher number of oxygenated defects and therefore Au NP are evenly distributed on all the tubes.

UV−vis−NIR spectra are shown in Figure 6. The van Hove singularities appear to be completely lost in **ox-SWNT**, whereas **Au-ox-SWNT** present the same characteristic peaks as **b-SWNT**. This effect suggests that electron transfer from the particles to the tubes occurs, restoring the available electrons for optical transitions. In fact, Charlier *et al.* reported the electron distribution for Au bonded to an oxidized vacancy at the CNT surface to be $0.2e^-$ transfer from the Au atom to the tube, which confirms our hypothesis.[36] Further support to this assumption is the reduction in the relative intensity of the satellite peak in the high binding energy of the C 1s peak. As discussed above, this effect can be associated to both preferential nucleation onto the oxygenated groups and charge transfer to the tube. The spectra lines of **Au-ox-SWNT** and **b-SWNT** cross at ~1000 nm, in the E_{11} semiconducting region. From this point a slightly higher absorbance of **b-SWNT** is observed while at E_{22} semiconducting and E_{11} metal the absorption intensity is higher for **Au-ox-SWNT**. These latter regimes might be more affected by the UV irradiation than the E_{11} semiconducting region, since this latter is more distant in energy. From this, we can say that

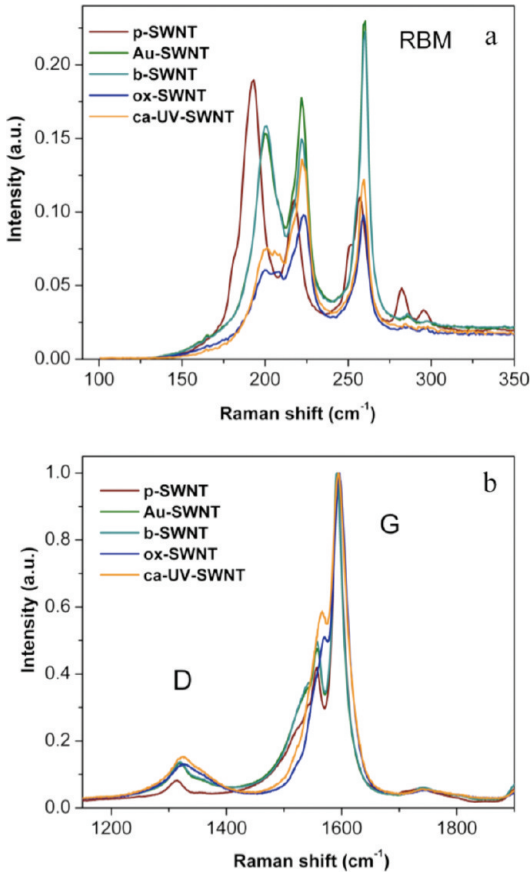

Figure 8. (a) D and G bands of the Raman spectra of SWNT samples, p-SWNT, Au-ox-SWNT, b-SWNT, ox-SWNT, and ca-UV-ox-SWNT. (b) Raman breathing mode (RBM) spectra of SWNT samples, p-SWNT, Au-ox-SWNT, b-SWNT, ox-SWNT, and ca-UV-ox-SWNT.

UV irradiation induces a faster nucleation of Au NP on metallic and thin semiconducting SWNT.

For **Au-ox-SWNT** composites produced at higher concentration of gold (1 and 3 mM), we observed after centrifugation that it is possible to obtain fractions of tubes with different amounts of Au NP deposited. Figure 7 shows the UV−vis−NIR spectra and a photograph of the different tubes in DMF. As can be noticed, the solution at the right side presents the typical color of SWNT diluted solution, nevertheless the presence of Au NP can be noticed in the UV spectra. The other fractions present different intensities of purple coloration originating from the higher concentration of Au NP. This fact can be corroborated by the intensity of the peak at 570 nm in the UV spectrum. The strong UV absorption of Au NP masked the characteristic van Hove singularities of SWNT before 1000 nm.

Finally, to investigate the nature of the interactions between Au NPs and SWNT, Raman spectra were recorded. Figure 8 displays the Raman response of **p-SWNT**, **ox-SWNT**, **Au-ox-SWNT**, **b-ox-SWNT**, and **ca-UV-ox-SWNT**.

The increase of the D band intensity at about 1320 cm^{-1} for the oxidized tubes clearly shows that treatment with nitric acid induces new defects on the nanotubes. The intensity of this band does not change too much with the other manipulations of the nanotubes indicating that there is a small variation of the number of defects. Some changes, which can be observed at about 1350 cm^{-1}, are usually considered to derive from the purification of the sample from carbonaceous materials. It is also possible to observe other variations in the region between 1500 and 1550 cm^{-1}, namely a decreasing of the intensity of the shoulder of the main G band. This region usually indicates the presence of metallic nanotubes and its decreasing can be related to some attack to this type of nanotubes. The intensity of this shoulder is recovered in particular for the nanotubes treated with Au nanoparticles, while treatment of **Au-ox-SWNT** with reducing agents, such as citrate, does not give the same result (see Figure 8a).

One can interpret this phenomenon considering that the oxidation of the nanotubes not only produces new functional groups on the tubes but it is a p-doping for the electronic structure of the nanotubes. Therefore, the possible role of the Au nanoparticles could be that of a donor agent, which alleviates the p-doping and regenerates the SWNT original electronic situation. This, however, does not mean that the nanotubes have lost their functional groups because the intensity of the D band is not significantly decreased.

Confirmation of these results comes from the analysis of the RBM region below 400 cm^{-1} (see Figure 8b). In these spectra, it is possible to see that the oxidation determines a decrease of both the bands above 280 cm^{-1} and those below 230 cm^{-1}. The highest wavenumber bands are related to semiconducting tubes (in particular (7,5) and (8,3)), and it is known that these small diameter nanotubes react more easily than others in a strong oxidation.[37] On the other hand the bands at lower wavenumbers can be related to large diameter metallic nanotubes ((12,3) and (13,1) at about 220 cm^{-1} and (13,4), (12,6), and (14,2) at about 195 cm^{-1}). The band at about 255 cm^{-1} can be related to semiconducting nanotubes ((9,4), (11,1,) and (9,3)) A recovery, in particular of the intensity of the metallic nanotubes, can be observed, although with an increased wavenumber with respect to the **p-SWNT**, for the **Au-ox-SWNT** and **b-SWNT** samples. The increased frequency is usually observed for functionalized nanotubes and the recovery of the intensity for the nanotubes treated with Au nanoparticles, can be related to a recovery of the electronic structure of these nanotubes. These observations confirm the conclusions reached in the G-band spectral region.

In conclusion, we have deposited Au NP on oxidized SWNT using UV light irradiation. Our experimental findings suggest that oxygenated groups covalently attached to SWNT are the nucleation sites for NP growth. Irradiation of the SWNT oxidized using nitric acid (**ox-SWNT**) at low $HAuCl_4$ loading resulted in the formation of small NP (~2 nm), while for increasing $HAuCl_4$ loading, both the growth factor and the size distribution af the NP are affected. The presence of different type and amount of oxygen groups grafted at the

MWNT surface and the catalytic activity of nanoscale gold particles under UV light irradiation can explain the broadening of the NP size distribution for increasing $HauCl_4$ loading. In SWNT oxidized using piranha solution (**cut-SWNT**), the amount of oxygen groups grafted is higher while the spread in the nature is smaller than in the **ox-SWNT** sample implying a narrower NP size distribution (11 nm). The increase in the thermal stability of the **Au-SWNT** composites suggests that NP nucleate on oxidized defects preventing further oxidation.

The observation that in dispersions of pristine (**p-MWNT**) and highly damage MWNT (**cut-MWNT**, 9 h in piranha solution) the Au NP grow in solution instead of growing attached at the tube surface indicates that both the efficient creation of electron−hole (e−h) pairs in the nanotube and the presence of oxygen groups grafted at the tube surface are necessary for the nucleation and growth of Au NP at the tube surface. Faster nucleation of Au NP was observed on metallic SWNT, this can be associated with a high probability of e−h pairs formation on this type of tubes. Separation of bare tubes (**b-SWNT**) from **Au-ox-SWNT** was achieved using dodecylthiol, which forms a self-assembled monolayer onto the Au-NP surface. TGA, UV−vis−NIR and Raman spectroscopy reveal a regeneration of the pristine SWNT properties in **Au-ox-SWNT** and **b-SWNT**.

METHODS

Oxidation of SWNT. A 300 mg portion of pristine SWNT (**p-SWNT**, HiPCO SWNT, Carbon Nanotechnology, Inc., lot no. R0496, www.cnanotech.com) was sonicated for 5 min in 300 mL of 2.6 M solution of nitric acid and refluxed for 48 h at 125 °C under magnetic stirring.[15] The solution was neutralized, filtered (Millipore JH 0.45 μm filter), and washed with deionized water. After that, the oxidized SWNT (**ox-SWNT**) were washed with methanol and dried in vacuo overnight (249 mg, 83%). Cut SWNT (**cut-SWNT**) were prepared placing **ox-SWNT** in piranha solution for 1 h and in a different experiment from 9 h at 22 °C following the previous reported work. To increase the dispersibility of **ox-SWNT**, sodium dodecyl sulfate (SDS, 1 wt %) was added in some cases (**SDS-ox-SWNT**) before $HAuCl_4$ loading and UV light irradiation.

Deposition of Gold NP on Carbon Nanotubes. A 10 mg portion of the **ox/cut SWNT** was sonicated in 10 mL of 1 M solution of methanol in water for 10 min. Citric acid solution in water (1.5 M) was used to adjust the pH = 1. $HAuCl_4$ was used as metal precursors (0.05, 1, and 3 mM). Water dispersions were deoxygenated with argon in order to avoid photo-oxidation of tubes. Solutions were irradiated with UV light (GE.R 500 W Helios Italquartz, 250−450 nm, λ_{max} = 360 nm) for intervals of 60 min under magnetic stirring. Control solutions were kept in daylight during the same time (**dl-Au-ox-SWNT**). Control samples were prepared following the same procedure described above but without any of the main component, such as citric acid, $HAuCl_4$, or methanol. Solutions were filtered (Millipore JH 0.45 μm filter), washed with deionized water, and dried under vacuum.

Separation of Au-ox-SWNT. For the separation of **Au-ox-SWNT** from **b-SWNT**, 10 mg of dry UV light synthesized **Au-ox-SWNT** composites prepared at low Au concentration in solution, were dispersed in DMF, and dodecylthiol was added in 1:1 volume ratio. Dispersions were sonicated until homogeneous solution were obtained and later were centrifuged for 1 h at 3000 rpm and kept overnight. Two clear liquid phases were observed and also two precipitated nanotube fractions, one at the bottom of the test tubes (**b-SWNT**) and the other (**Au-ox-SWNT**) at the interface of DMF−dodecylthiol ($\rho_{dodecylthiol}$ = 0.85 g/mL and ρ_{DMF} = 0.944 g/mL). The fractions were separated, filtered, and washed thoroughly. The collected nanotubes were dried in vacuo overnight. After that the two fractions (**b-SWNT** and **Au-ox-SWNT**) where dispersed in DMF for their characterization. In samples with higher Au concentration, the **Au-ox-SWNT** fraction was centrifuged again and washed in methanol in order to remove the remaining dodecylthiol. Samples were redispersed in DMF for further characterization.

The given names to the different treated CNT used in this study are summarized in Table 1.

Sample Characterization. For UV−vis−NIR characterization (1 cm quartz cuvettes on a Varian Cary 5000 spectrophotometer), 2 mg of each compound was dispersed in 10 mL of DMF, sonicated for 10 min and centrifuged at 3000 rpm for 20 min. Raman spectra were recorded with an Invia Renishaw microspectrometer equipped with a He Ne laser at 633 nm. Tapping-mode AFM analysis measurements of the mica substrates were carried out in air at 298 K, using a Nanoscope IIIa (Digital Instruments Metrology Group, USA) instrument. The tips used in all measurements were phosphorus-doped silicon cantilevers (T = 20−80 mm, L = 115−135 mm, f = 200−400 kHz, k = 20−80 N m^{-1}, VEECO, USA) at a resonant frequency of *ca*. 290 kHz. Thermogravimetric analyses (TGA) of approximately 1 mg of each compound were recorded on a TGA Q500 (TA Instruments) under N_2 or air by equilibrating at 100 °C, and following a ramp of 10 °C/min up to 1000 °C. Transmission electron microscopy analyses were performed on a TEM Philips EM208, using an accelerating voltage of 100 kV. For the sample preparation 0.1 mg of the different compounds was dispersed in 1 mL of solvent, and one drop of this solution was deposited on a TEM grid (200 mesh, nickel, carbon only). Analysis of individual metal particles was performed by high-resolution TEM using a Philips CM30 FEG microscope, operated at 200 kV electron energy. The chemical composition of the samples was examined through XPS analysis carried out in a VG-ESCALAB 220iXL instrument equipped with an Al Kα monochromatized X-ray beam. The X-ray emission energy was 25 W with 15 kV accelerating voltage focused to a spot of 250 × 1000 μm. Typical operating pressures were better than 10^{-9} Torr. The emitted electrons were detected by a hemispherical analyzer at fixed pass energy of 20 eV for the high-resolution spectra for all specimens. The takeoff angle was generally 90° (the angle between the specimen surface and the direction of photoelectrons to the detector).

TABLE 1. Summary of the Differently Treated CNT

sample name	type of CNT
p-SWNT	pristine HiPCO SWNT
ox-SWNT	SWNT oxidized in nitric acid
cut-SWNT	ox-SWNT treated in piranha solution
Au-ox-SWNT	ox-SWNT after gold nanoparticles deposition
Au-cut-SWNT	cut-SWNT after gold nanoparticles deposition
Au-SDS-ox-SWNT	ox-SWNT dispersed in sodium dodecyl sulfate solution
b-SWNT	purified ox-SWNT after separation from Au-ox-SWNT
dl-Au-ox-SWNT	ox-SWNT kept in day light at the same condition of Au-ox-SWNT
ca-UV-ox-SWNT	ox-SWNT treated with UV-light in citric acid solution
Au-MWNT	pristine MWNT treated in the same conditions as Au-SWNT

Acknowledgment. This work was financially supported by the University of Trieste, INSTM, Italian Ministry of Education MIUR (cofin Prot. 20085M27SS and Firb RBIN04HC3S), and the Belgian Program on Interuniversity Attraction Pole (PAI 6/08), ARC-UMH. We are very grateful to Prof. Paolo Fornasiero and Dr. Valentina Gombac, University of Trieste, for advice and helpful discussion.

REFERENCES AND NOTES

1. Cherukuri, P.; Gannon, C. J.; Leeuw, T. K.; Schmidt, H. K.; Smalley, R. E.; Curley, S. A.; Weisman, R. B. Mammalian Pharmacokinetics of Carbon Nanotubes Using Intrinsic

Near-Infrared Fluorescence. *Proc. Natl. Acad. Sci.* **2006**, *103*, 18882–18886.
2. Kostarelos, K.; Bianco, A.; Prato, M. Promises, Facts and Challenges for Carbon Nanotubes in Imaging and Therapeutics. *Nat. Nanotechnol.* **2009**, *4*, 627–633.
3. Katz, E.; Willner, I. Biomolecule-Functionalized Carbon Nanotubes: Applications in Nanobioelectronics. *Chem. Phys. Chem.* **2004**, *5*, 1084–1104.
4. Lee, J. U. Photovoltaic Effect in Ideal Carbon Nanotube Diodes. *Appl. Phys. Lett.* **2005**, *87*, 073101-1−073101-3.
5. Carlson, L. J.; Krauss, T. D. Photophysics of Individual Single-Walled Carbon Nanotube. *Acc. Chem. Res.* **2008**, *41*, 235–243.
6. Bandow, S.; Asaka, S.; Saito, Y.; Rao, A. M.; Gregorian, L.; Richter, E.; Ekunel, P. C. Effect of the Growth Temperature on the Diameter Distribution and Chirality of Single-Walled Carbon Nanotubes. *Phys. Rev. Lett.* **1998**, *80*, 3779–3782.
7. Gabor, N. M.; Zhong, Z.; Bosnick, K.; Park, J.; McEuen, P. L. Extremely Efficient Multiple Electron−Hole Pair Generation in Carbon Nanotubes Photodiodes. *Science* **2009**, *325*, 1367–1371.
8. (a) Linsebigler, A. L.; Lu, G. Q.; Yates, J. T. Photocatalysis on TiO_2 Surfaces: Principles, Mechanism, and Selected Results. *Chem. Rev.* **1995**, *95*, 735–758. (b) Hamon, M. A.; Sttensaas, K. L.; Sugar, M. A.; Tumminello, K. C.; Allred, A. K. Reacting Soluble Singled-Walled Carbon Nanotubes with Singlet Oxygen. *Chem. Phys. Lett.* **2007**, *447*, 1–4.
9. Alvarez, N. T.; Kittrell, C.; Schmith, H. K.; Hauge, R. H.; Engel, P. S.; Tour, J. M. Selective Photochemical Funtionalization of Surfactant-Dispersed Singled-Walled Carbon Nanotubes in Water. *J. Am. Chem. Soc.* **2008**, *130*, 14227–14233.
10. Mikó, Cs.; Milas, M.; Seo, J. W.; Gáal, R.; Kulik, A.; Forró, L. Effect of Ultraviolet Light Irradiation on Macroscopic Singled-Walled Carbon Nanotubes Bundles. *Appl. Phys. Lett.* **2006**, *88*, 151905–151907.
11. Kong, J.; Chapline, M. G.; Dai, H. Functionalized Carbon Nanotubes for Molecular Hydrogen Sensors. *Adv. Mater.* **2001**, *13*, 1384–1386.
12. Che, B.; Lakshmi, B. B.; Martín, C. R.; Fisher, E. R. Metal-Nanocluster-Filled Carbon Nanotubes: Catalytic Properties and Possible Application in Electrochemical Energy Storage and Production. *Langmuir* **1999**, *15*, 750–758.
13. Li, W. Z.; Liang, C. H.; Zhou, W. J.; Qiu, J. S.; Zhou, Z. H.; Sun, G. Q.; Xin, Q. Preparation and Characterization of Multiwalled Carbon Nanotubes Supported Platinium for Cathode Catalyst of Direct Methanol Fuel Cells. *J. Phys. Chem. B* **2003**, *107*, 6292–6299.
14. Bell, A. T. The Impact of Nanoscience on Heterogeneous Catalysis. *Sciences* **2003**, *299*, 1688.
15. Yang, S.; Wang, Y.; Wang, Q.; Zhang, R.; Ding, B. UV Irradiation Induced Formation of Gold Nanoparticles at Room Temperature: The Case of pH Values. *Colloids Surf., A* **2007**, *301*, 174–183.
16. Lui, J.; Rinzler, A. G.; Dai, H.; Hafner, J. H.; Bradley, R. K.; Boul, P. J.; Lu, A.; Iverson, T.; Shelimov, K.; Huffman, C. B.; *et al.* Fullerene Pipes. *Science* **1998**, *280*, 1253–1256.
17. Ziegler, K. J.; Gu, Z.; Peng, H.; Flor, E. L.; Hauge, R. H.; Smalley, R. E. Controlled Oxidative Cutting of Singled-Walled Carbon Nanotubes. *J. Am. Chem. Soc.* **2005**, *127*, 1541–1547.
18. Georgakilas, V.; Gournis, D.; Tzitzios, V.; Pasquato, L.; Guldi, D. M.; Prato, M. Decoration of Carbon Nanotubes with Metal and Semiconductor Nanoparticles. *J. Mater. Chem.* **2007**, *17*, 2679–2694.
19. Bittencourt, C.; Felten, A.; Douhard, B.; Ghijsen, J.; Johnson, R. L.; Drube, W.; Pireaux, J.-J. Photoemission Studies of Gold Clusters Thermally Evaporated on Multiwalled Carbon Nanotubes. *Chem. Phys.* **2006**, *328*, 385–391.
20. Felten, A.; Ghijsen, J.; Pireaux, J.-J.; Johnson, R. L.; Whelan, C. M.; Liang, D.; Van Tendeloo, G.; Bittencourt, C. Effect of Oxygen rf-Plasma on Electronic Properties of Carbon Nanotubes. *J. Phys. D* **2007**, *40*, 7379–7382.
21. (a) Ago, H.; Kugler, T.; Cacialli, F.; Salaneck, W. R.; Shaffer, M. S. P.; Friend, R. H.; Windle, A. H. Work Functions and Surface Functional Groups of Multiwalled Carbon Nanotubes. *J. Phys. Chem. B* **1999**, *103*, 8116–8121. (b) Pirlot, C.; Willems, I.; Fonseca, A.; Nagy, J. B.; Delhalle, J. Preparation and Characterization of Carbon Nanotube/Polyacrylonitrile Composites. *Adv. Eng. Mater.* **2002**, *4*, 109–114.
22. Buttner, M.; Oelhafen, P. XPS Study on the Evaporation of Gold Submolayers on Carbon Surfaces. *Surf. Sci.* **2006**, *600*, 1170–1177.
23. Suarez-Martinez, I.; Bittencourt, C.; Ke, X.; Felten, A.; Pireaux, J. J.; Ghijsen, J.; Drube, W.; Van Tendeloo, G.; Ewels, C. P. Probing Interactions between Gold Nanoparticles and Oxygen Functionalized Carbon Nanotubes. *Carbon* **2009**, *47*, 1549–1554.
24. Wallace, W. T.; Min, B. K.; Goodman, D. W. The Stabilization of Supported Gold Clusters by Surface Defects. *J. Mol. Catal. C* **2005**, *228*, 3–10.
25. Ajayan, P. M.; Ebbesen, T. W.; Ichihashit, T.; Tanigaki, K.; Hiura, H. Opening Carbon Nanotubes with Oxygen and Implications for Filling. *Nature* **1993**, *362*, 522–525.
26. Choi, H. C.; Shim, M.; Bangsaruntip, S.; Dai, H. Spontaneous Reduction of Metal Ions on the Side Walls of Carbon Nanotubes. *J. Am. Chem. Soc.* **2002**, *124*, 9058–9059.
27. Ziegler, K. J.; Gu, Z.; Peng, H.; Flor, E. L.; Hauge, R. H.; Smalley, R. E. Controlled Oxidative Cutting of Single-Walled Carbon Nanotubes. *J. Am. Chem. Soc.* **2005**, *127*, 1541–1547.
28. Hartling, T.; Seidenstucker, A.; Olk, P.; Plettl, A.; Ziemann, P.; Eng, M. L. Controlled Photochemical Particle Growth in Two-Dimensional Ordered. *Nanotechnology* **2010**, *21*, 145309.
29. Zhang, R.; Wang, Q.; Zhang, L.; Yang, S.; Yang, Z.; Ding, B. The Growth of Uncoated Gold Nanoparticles in Multiwalled Carbon Nanotubes. *Coll. Surf., A* **2008**, *312*, 136–141.
30. Rosca, I. D.; Watari, F.; Uo, M; Akasaka, T. Oxidation of Multiwalled Carbon Nanotubes by Nitric Acid. *Carbon* **2005**, *43*, 3124–3131.
31. Santhanam, V.; Liu, J.; Agarwal, R.; Andres, R. P. Self-Assembly of Uniform Monolayer Arrays of Nanoparticles. *Langmuir* **2003**, *19*, 7881–7887.
32. Juárez, B. H.; Klinke, C.; Kornowski, A.; Weller, H. Quantum Dot Attachment and Morphology Control by Carbon Nanotubes. *Nano Lett.* **2007**, *7*, 3564–3568.
33. Li, X.; Nie, J.; Zhang, J.; Li, H.; Liu, Z. Labelling Defects of Single-Walled Carbon Nanotubes Using Titanium Oxide Nanoparticles. *J. Phys. Chem. B* **2003**, *107*, 2453–2458.
34. Joseph, Y.; Besnard, I.; Rosenberger, M.; Guse, B.; Nothofer, H.-G.; Wessels, J. M.; Wild, U.; Knop-Gericke, A.; Su, D.; Schlogl, R.; *et al.* Self-Assembled Gold Nanoparticle/Alkanedithiol Films: Preparation, Electron Microscopy, XPS-Analysis Charge Transport, Vapor-Sensing Properties. *J. Phys. Chem. B* **2003**, *107*, 7406–7413.
35. Johnson, S. R.; Evans, S. D.; Brydson, R. Influence of a Terminal Funcionality on the Physical Properties of Surfactant-Stabilized Gold Nanoparticles. *Langmuir* **1998**, *14*, 6639–6647.
36. Charlier, J-C; Arnaud, L; Avilov, I. V.; Delgado, M.; Demoisson, F.; Espinosa, E. H.; Ewels, C. P.; Felten, A.; Guillot, J.; Ionescu, R. Carbon Nanotubes Ramdonly Decorated with Gold Clusters: From Nano2hybrid Atomic Structures to Gas Sensing Prototypes. *Nanotechnology* **2009**, *20*, 375501.
37. Chiang, I. W.; Brinson, B. E.; Huang, A. Y.; Willis, P. A.; Bronikowski, M. J.; Margrave, J. L.; Smalley, R. E.; Hauge, R. H. Purification and Characterization of Single-Walled Carbon Nanotubes (SWNTs) Obtained from Gas-Phase Decomposition of CO (HipCo process). *J. Phys. Chem. B* **2001**, *105*, 8297–8301.